Ab initio studies of thermodynamic and electronic properties of phosphorene nanoribbons

Ashwin Ramasubramaniam*
Department of Mechanical and Industrial Engineering, University of Massachusetts Amherst, Amherst, Massachusetts 01003, USA

Andre R. Muniz†
Department of Chemical Engineering, Universidade Federal do Rio Grande do Sul, Rua Luiz Englert s/n, 90040-040 Porto Alegre, Rio Grande do Sul, Brazil

(Received 11 June 2014; revised manuscript received 6 August 2014; published 20 August 2014)

We present a density functional theory study of the thermodynamic and electronic properties of phosphorene nanoribbons. We consider a variety of terminations and reconstructions of ribbon edges, both with and without hydrogen passivation, and calculate an *ab intio* phase diagram that identifies energetically preferred edges as a function of temperature and hydrogen partial pressure. These studies are also accompanied by detailed electronic structure calculations from which we find that ribbons with hydrogenated edges are typically direct gap semiconductors with fundamental gaps that are in excess of phosphorene, the gaps varying inversely with ribbon width. In contrast, ribbons with bare or partially passivated edges either have metallic edges or are semiconducting with band gaps that are smaller than those of their hydrogenated counterparts due to the appearance of midgap edge states. Overall, our studies provide a basis for tailoring the electronic properties of phosphorene nanoribbons by controlling the edge termination via processing conditions (temperature and hydrogen partial pressure) as well as by confinement of carriers via control over ribbon width.

DOI: 10.1103/PhysRevB.90.085424 PACS number(s): 81.07.−b

I. INTRODUCTION

Black phosphorus—the most stable allotrope of phosphorus—is a layered material in which puckered atomic sheets are held together by van der Waals forces [1–3]. It has long been known that bulk black phosphorus is a narrow-gap semiconductor with a band gap of approximately 0.30–0.35 eV and large but rather anisotropic carrier mobilities [3,4]. Exfoliated black phosphorus, an individual sheet of which has been dubbed phosphorene, has now become one of the newest entrants in the field of two-dimensional materials for nanoscale electronics. Recent experiments have already demonstrated potential uses for few-layer black phosphorus in field-effect transistors [5,6] and complementary metal-oxide semiconductor circuits [7]. Both experiment [7] and theory [3,4,7,8] show that the band gap in black phosphorus is sensitive to the number of layers and reaches a maximum value of ∼1 eV in the monolayer limit [7]. Furthermore, the band gap is also sensitive to interlayer spacing (applied pressure) [3] and can be tuned systematically from semiconducting to metallic with decreasing interlayer spacing [8]. In addition to layered structures, black phosphorus has also been studied theoretically in the form of nanotubes [9,10], which are predicted to exist as stable structures with semiconducting properties irrespective of chirality [10]. A few electronic structure studies on phosphorene nanoribbons have appeared recently [11–15], but none that properly take into account the thermodynamic stability of edges, which is a necessary condition for the existence of such ribbons. These studies consider phosphorene nanoribbons (PNRs) with two types of edges (zigzag and armchair), either bare or functionalized (with different species), and show that armchair PNRs are semiconducting while zigzag PNRs are either semiconducting or metallic depending on edge termination. One of these studies [13] additionally presents PNRs with a zigzag-edge variant (termed "cliff"), which are semiconducting. Formation/cohesive energies have been computed in some of these studies [11,13], suggesting that H-passivated PNRs are more stable than bare ones and that zigzag-PNRs are more stable than armchair ones for the same width.

The purpose of this article is to present a detailed study of the thermodynamic and electronic properties of phosphorene nanoribbons, taking into account a variety of edge terminations and reconstructions not previously reported, and clearly establishing their energetic ordering over a wide range of relevant processing parameters. We consider phosphorene nanoribbons with bare as well as hydrogenated edges and calculate an *ab initio* phase diagram that identifies the energetically preferred candidates as a function of temperature and hydrogen partial pressure. Our thermodynamic studies are also accompanied by detailed electronic structure analyses from which we find that all ribbons with hydrogenated edges are semiconducting with fundamental band gaps that are larger than pristine phosphorene due to quantum confinement. Ribbons with bare edges can be either semiconducting or metallic, the metallicity arising from dangling-bond edge states. Collectively, our thermodynamic and electronic structure analyses provide a detailed map for potential synthesis of PNRs for nanoscale electronics.

II. METHODS

Our calculations were all performed using density functional theory (DFT) as implemented in the Vienna *Ab Initio* Package (VASP) [16]. Core and valence electrons were treated using the projector augmented wave method [17,18] while electron exchange and correlation was treated using the Perdew-Burke-Ernzerhof (PBE) [19] form of the generalized-gradient approximation. From convergence studies, a plane-wave cutoff of 500 eV was chosen. The Brillouin zone was

*ashwin@engin.umass.edu
†amuniz@enq.ufrgs.br

sampled with a Γ-centered k-point mesh using a mesh density equivalent to a 12×9×1 mesh for a unit cell of monolayer phosphorene. Structural relaxations were performed with a force tolerance of 0.01 eV/Å. To accelerate electronic convergence, a 0.05 eV Gaussian smearing of the Fermi surface was employed. Γ-point vibrational calculations were performed using the density functional perturbation theory approach implemented in VASP.

III. RESULTS AND DISCUSSION

Figure 1(a) shows a schematic of a phosphorene sheet whose characteristic buckled structure arises from the sp^3 hybridization of phosphorus atoms. The zigzag, in-plane bonds are aligned with the low-mobility direction for carrier transport whereas the orthogonal, buckled armchair direction is associated with high carrier mobility [3,7,20]. Figure 1(b) displays a top view of the phosphorene sheet with three distinct directions of the nanoribbon edges considered here: the armchair (AC) edge; two variants of the zigzag edge obtained by either cutting all of the in-plane (ZZ′) or the out-of-plane (ZZ) P-P bonds; and a third type of edge (θ_{54}—oriented approximately at 54° to the zigzag direction), which is obtained by cutting only one specific orientation of in-plane P-P bonds. Other high-index edges are not considered here; a more complete Wulff plot will be reported elsewhere.

Figures 2 and 3 display sample relaxed structures of nanoribbons with armchair, θ_{54}, and zigzag edges. For the AC and θ_{54} cases, the edge P atoms each have a single dangling bond, which can be passivated by a single H atom (denoted AC_H and $\theta_{54,H}$; Fig. 2); this is compatible with the preferred sp^3 hybridization of P atoms in black phosphorus and results in

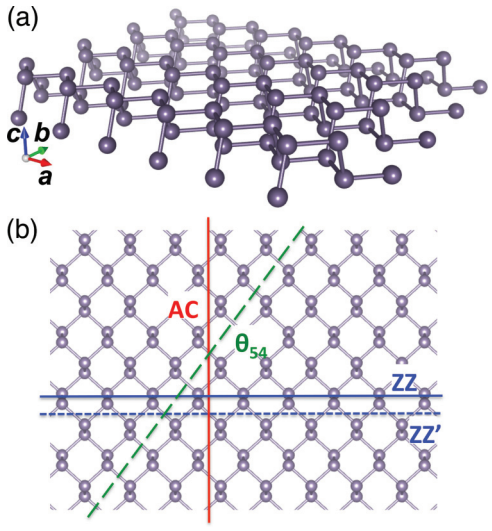

FIG. 1. (Color online) (a) Atomic model showing the puckered structure of a black phosphorus monolayer. The zigzag direction is oriented along the a axis. (b) Top view of a monolayer indicating directions of cuts that result in the various edge terminations (armchair, AC; 54° edge, θ_{54}; zigzag, ZZ and ZZ′) of the nanoribbons considered here. The zigzag variants are obtained by either cutting the out-of-plane P-P bonds (ZZ) or the in-plane ones (ZZ′).

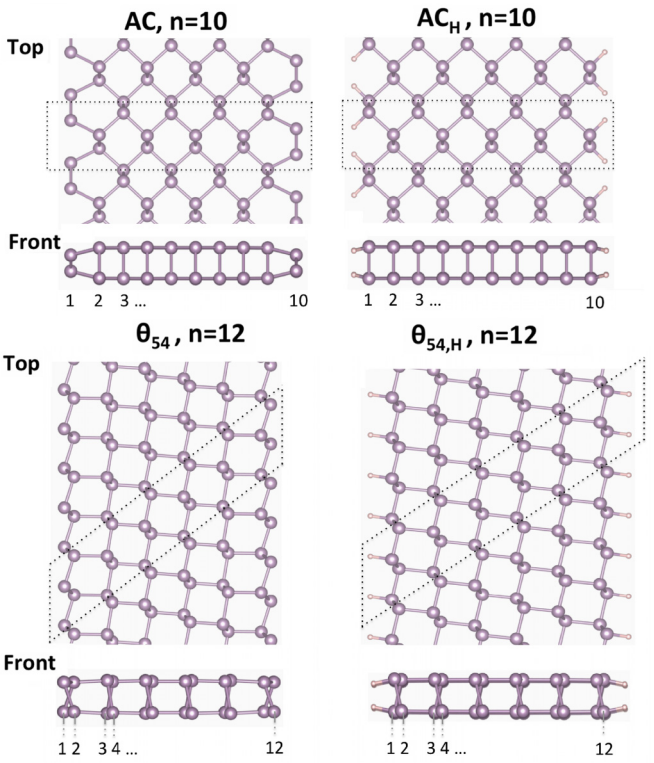

FIG. 2. (Color online) Examples of relaxed structures of bare and hydrogenated armchair (AC, AC_H) and 54° edge (θ_{54},$\theta_{54,H}$) nanoribbons. The numbering scheme for the labeling of ribbons is also indicated. The unit cells (excluding vacuum) are represented by dotted lines.

mechanically stable nanoribbons as determined from a Γ-point vibrational analysis. For bare edges, a vibrational analysis reveals that the armchair edge is mechanically stable whereas the θ_{54} edge has multiple large imaginary modes rendering it unstable to long wavelength perturbations; the bare θ_{54} edge is therefore not considered further. The zigzag edges show a richer variety of edge terminations and reconstructions as displayed in Fig. 3. The ZZ edge, obtained by cutting the out-of-plane P-P bonds, results in edge P atoms each with a single dangling bond, which can be passivated by a single H atom (ZZ_H structure) to retain the P sp^3 hybridization; both the ZZ and ZZ_H edges are mechanically stable. The ZZ′ edge, obtained by cutting the in-plane P-P bonds, however, results in P edge atoms with two dangling bonds each. It might be expected that neighboring P-P atoms along such an edge could form a 2×1 dimer reconstruction (ZZ'_{2x1}) to eliminate one dangling bond and thus reduce the edge energy; the remaining dangling bond could then be passivated by a single H atom ($ZZ'_{2x1,H}$). Alternatively, the two dangling bonds of the edge P atoms could be partially (ZZ'_{1H}) or fully (ZZ'_{2H}) passivated by H atoms without any other edge reconstructions.

The edge energies for the various nanoribbon edges described above are listed in Table I. Briefly, to obtain the energy of a particular edge termination, we performed energy minimization calculations while relaxing both the atomic positions and the single periodic vector of various nanoribbons. The widths of the nanoribbons were systematically increased

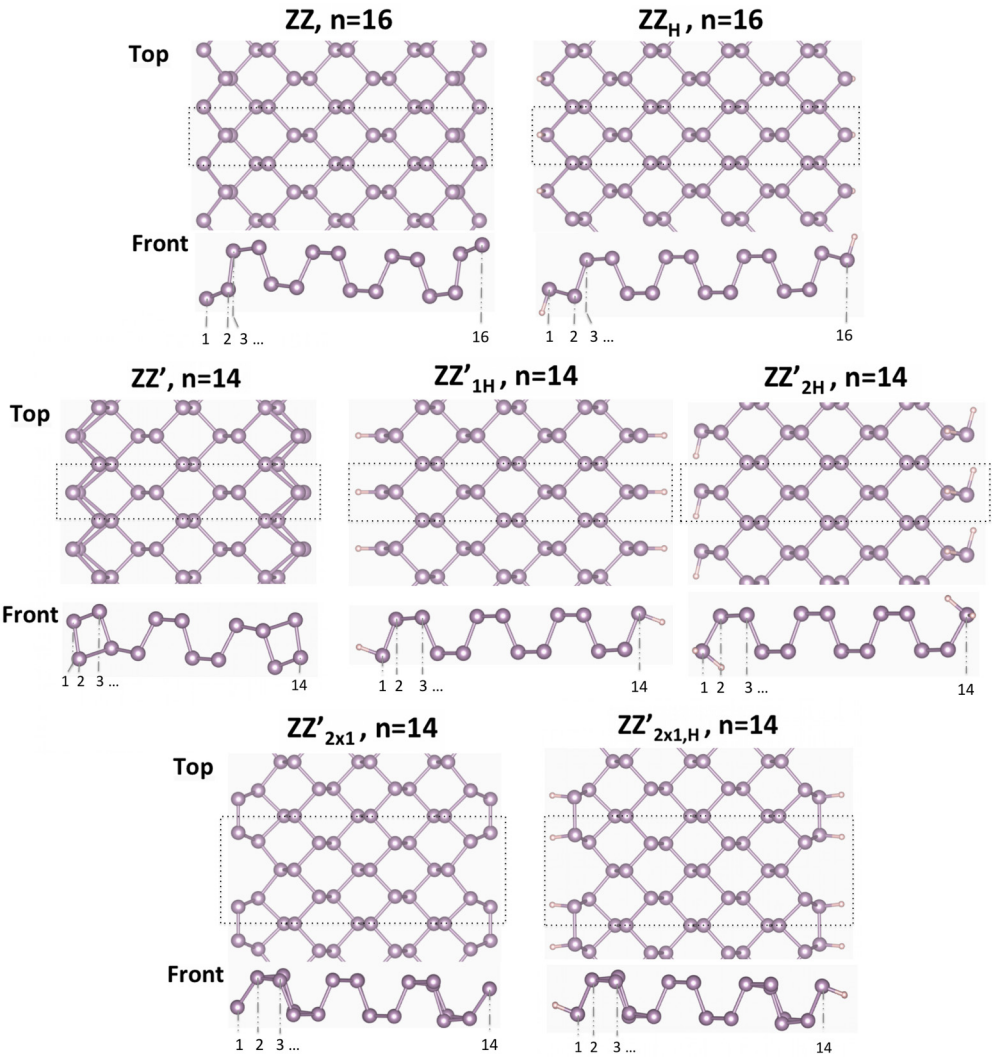

FIG. 3. (Color online) Examples of relaxed structures of ZZ and ZZ′ variants of bare and hydrogenated zigzag nanoribbons. The ZZ′ variant, in particular, supports single and double hydrogenation of edges. The ZZ′ edge also supports a 2×1 dimer edge-reconstruction which can further be singly hydrogenated. The numbering scheme for the labeling of ribbons is indicated as are the unit cells (excluding vacuum), which are represented by dotted lines.

until the excess energy was insensitive (<5 meV/Å) to any further increase in width; this procedure eliminates system-size dependence of edge energies. The edge energies were then calculated as

$$\gamma_{\text{bare}}(T) = (G_{\text{ribbon}}(T) - N_{\text{P}}\mu_P(T))/2L, \tag{1}$$

$$\gamma_{\text{H-term}}(T,p) = \left(G_{\text{ribbon}}(T) - N_{\text{P}}\mu_P(T) - N_{\text{H}}\frac{\mu_{\text{H}_2}(T,p)}{2}\right)\Big/2L, \tag{2}$$

for bare and hydrogenated ribbons of (relaxed) length L, respectively. In the above equations, $G_{\text{ribbon}}(T)$ is the Gibbs free energy of the nanoribbon, $\mu_P(T)$ is the chemical potential (specific Gibbs free energy) of a P atom in monolayer black phosphorus, $\mu_{\text{H}_2}(T,p)$ is the chemical potential of a hydrogen molecule in the gas phase, N_{P} is the number of P atoms in the ribbon, N_{H} is the number of H atoms, T is the temperature, and p is the partial pressure of hydrogen gas. For zero temperature calculations reported in Table I, the chemical potentials are all simply DFT total energies. From Table I, we see that among the bare edges, the dimer-reconstructed edge, ZZ′$_{2x1}$,

TABLE I. Edge energies in eV/Å for bare and hydrogenated nanoribbons at 0 K. The nomenclature of ribbons is indicated in Figs. 2 and 3.

Bare				Hydrogenated					
AC	ZZ	ZZ′	ZZ′$_{2x1}$	AC$_H$	$\theta_{54,H}$	ZZ$_H$	ZZ′$_{1H}$	ZZ′$_{2H}$	ZZ′$_{2x1,H}$
0.27	0.21	0.37	0.16	0.01	0.01	0.01	0.20	0.11	0.03

is energetically most preferred. In general, H passivation of dangling bonds leads to edge energies lower than those for the bare cases with the exception of the ZZ'_{1H} edge, which is higher in energy than the ZZ'_{2x1} case. Overall, the AC_H, $\theta_{54,H}$, and ZZ_H edges are all nearly degenerate at 0 K; changes in the hydrogen chemical potential due to finite temperature effects and/or changes in the H_2 partial pressure can lift this near degeneracy as seen further below.

For the above thermodynamic results to be relevant to experiments though, it is necessary to have some estimate of the effect of nonzero temperatures as well as hydrogen partial pressure on preferred edge terminations. To accomplish this, we follow standard techniques of *ab initio* thermodynamics [21,22]. First, the hydrogen chemical potential (μ_{H_2}) can be calculated as the sum of translational (μ_{trans}), rotational (μ_{rot}), vibrational (μ_{vib}), and electronic (μ_{elec}) free energies. These individual components can in turn be calculated as [22]

$$\mu_{trans} = -k_B T \ln\left[\left(\frac{m}{2\pi\hbar^2}\right)^{3/2}\frac{(k_B T)^{5/2}}{p}\right], \quad (3)$$

$$\mu_{rot} = -k_B T \ln\left(\frac{k_B T}{\sigma^{sym} B_0}\right), \quad (4)$$

$$\mu_{vib} = \frac{\hbar\omega_0}{2} + k_B T \ln\left[1 - \exp\left(-\frac{\hbar\omega_0}{k_B T}\right)\right], \quad (5)$$

$$\mu_{elec} = E_{H_2} - k_B T \ln(I^{spin}), \quad (6)$$

where k_B and $\hbar$ are the Boltzmann constant and the Planck constant, respectively; m is the mass of the H_2 molecule, $\sigma^{sym} = 2$ is a symmetry number enumerating its indistinguishable orientations, B_0 is its rotational constant, and I^{spin} is the electronic spin degeneracy of its ground state; T and p are the temperature and partial pressure of H_2 gas; ω_0 is the vibrational frequency of the H_2 molecule, $\hbar\omega_0/2$ being the contribution from this mode to the zero-point energy (ZPE); and E_{H_2} is the total energy of the H_2 molecule. Combining the above results, the hydrogen chemical potential may be written in the form

$$\mu_{H_2}(T,p) = E_{H_2} + \frac{\hbar\omega_0}{2} - k_B T\left\{\ln\left[\left(\frac{m}{2\pi\hbar^2}\right)^{3/2}\frac{(k_B T)^{5/2}}{p}\right] + \ln\left(\frac{k_B T}{\sigma^{sym} B_0}\right) - \ln\left[1 - \exp\left(-\frac{\hbar\omega_0}{k_B T}\right)\right] + \ln(I^{spin})\right\} \quad (7)$$

$$\equiv E_{H_2} + E_{ZPE} + \Delta\mu_{H_2}(T,p^0) + k_B T \ln\left(\frac{p}{p^0}\right), \quad (8)$$

where p^0 is the reference partial pressure of H_2 gas. When expressed in the form of Eq. (8) [21–23], only E_{H_2} and E_{ZPE} need be calculated with DFT while $\Delta\mu_{H_2}(T,p^0)$ can be obtained from standard thermochemical tables [24]. However, since the available thermochemical data for H_2 gas are only valid for temperatures in excess of 298 K [24], we have chosen to retain the *ab initio* approach [Eq. (7)] in our calculations to span temperatures down to 0 K; as validation of the *ab initio* approach, we have checked that the chemical potential obtained from our calculations is in near perfect agreement

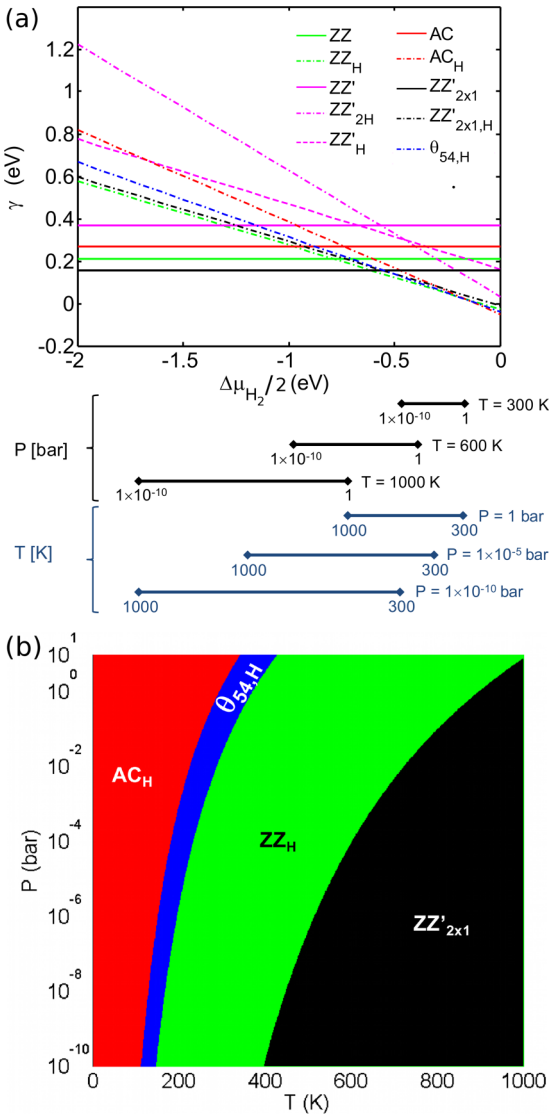

FIG. 4. (Color online) (a) Free energy, γ, of various edge terminations as a function of hydrogen chemical potential, $\Delta\mu_{H_2}/2$ [defined in Eqs. (7) and (8)]. Solid lines below the figure indicate the ranges of chemical potentials spanned by specific temperatures/partial pressures of H_2. (b) T-P phase diagram for nanoribbon edge terminations.

with that obtained from thermochemical data within the range of 298–1000 K [25]. Second, we require the Gibbs free energies of the solid phases to be calculated, which is much more demanding as these require calculation of the phonon density of states followed by an integration over the frequency spectrum. However, since the Gibbs free energies of the solid phases only enter as *energy differences*, we can expect significant cancellation of temperature-dependent terms with errors being of the same order as the accuracy as the numerical method [21,22]. Thus, the Gibbs free energies of the solid phases in Eqs. (1) and (2) can be replaced by 0 K DFT total energies; any temperature and pressure dependence now only enters through the hydrogen chemical potential.

Figure 4(a) displays a comprehensive plot of the edge free energies for all nanoribbon terminations considered here

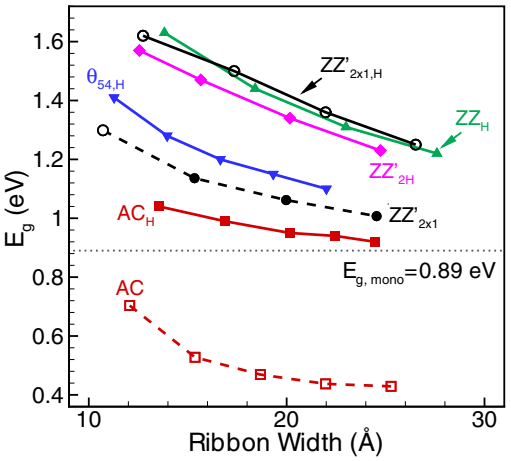

FIG. 5. (Color online) Fundamental band gap, E_g, of various nanoribbons as a function of ribbon width. Solid and dashed lines represent ribbons with hydrogenated and bare edges, respectively. Solid and empty symbols indicate direct and indirect band gaps, respectively. For reference, the DFT band gap of monolayer black phosphorus ($E_{g,\mathrm{mono}} = 0.89$ eV) is indicated by the horizontal dotted line.

from which one may read off not only the lowest energy edge termination but also the relative ordering of edge terminations as a function of hydrogen chemical potential; the chemical potential is more readily translated in practice as corresponding temperature and partial pressure, which are also displayed in this figure. The same data can be used to construct a phase diagram in T-P space as shown in Fig. 4(b). From this phase diagram, we readily notice that hydrogenated edges are consistently preferred at low temperatures relative to bare ones. It is only at elevated temperatures that we observe the emergence of the dimer-reconstructed (bare) zigzag edge, ZZ'_{2x1}, as the preferred phase. At room temperature, the ZZ_H phase is dominant over a very wide range (∼8 orders of magnitude) of hydrogen partial pressures. It is worth reemphasizing that we have only considered a select number of edge terminations here and, while the low Miller index edges are likely the most relevant ones, higher Miller index edges should also be considered to produce a more complete phase diagram.

Having established the stability and energetic ordering of ribbon edge terminations, we now turn our attention to the electronic structure of PNRs. It is well known that DFT underestimates band gaps in materials. For bulk black phosphorus, the experimentally measured gap is 0.30–0.35 eV whereas DFT calculations with the PBE functional predict gaps of 0.08 eV [26]. For phosphorene, we find a PBE band gap of 0.89 eV that is direct at the Γ point; Du *et al.* [27] reported a band gap of 0.75 eV using the PW-91 generalized gradient approximation (GGA) functional, Liu *et al.* [7] reported a band gap of 1.0 eV using the HSE06 hybrid functional, and Qiao *et al.* [28], reported a gap of ∼1.5 eV using the hybrid HSE06 and the modified Becke-Johnson meta-GGA functionals. The optical gap of phosphorene has been measured from photoluminescence experiments to be 1.45 eV [7], which should be a lower bound on the quasiparticle gap as excitonic effects ought be appreciable in the monolayer

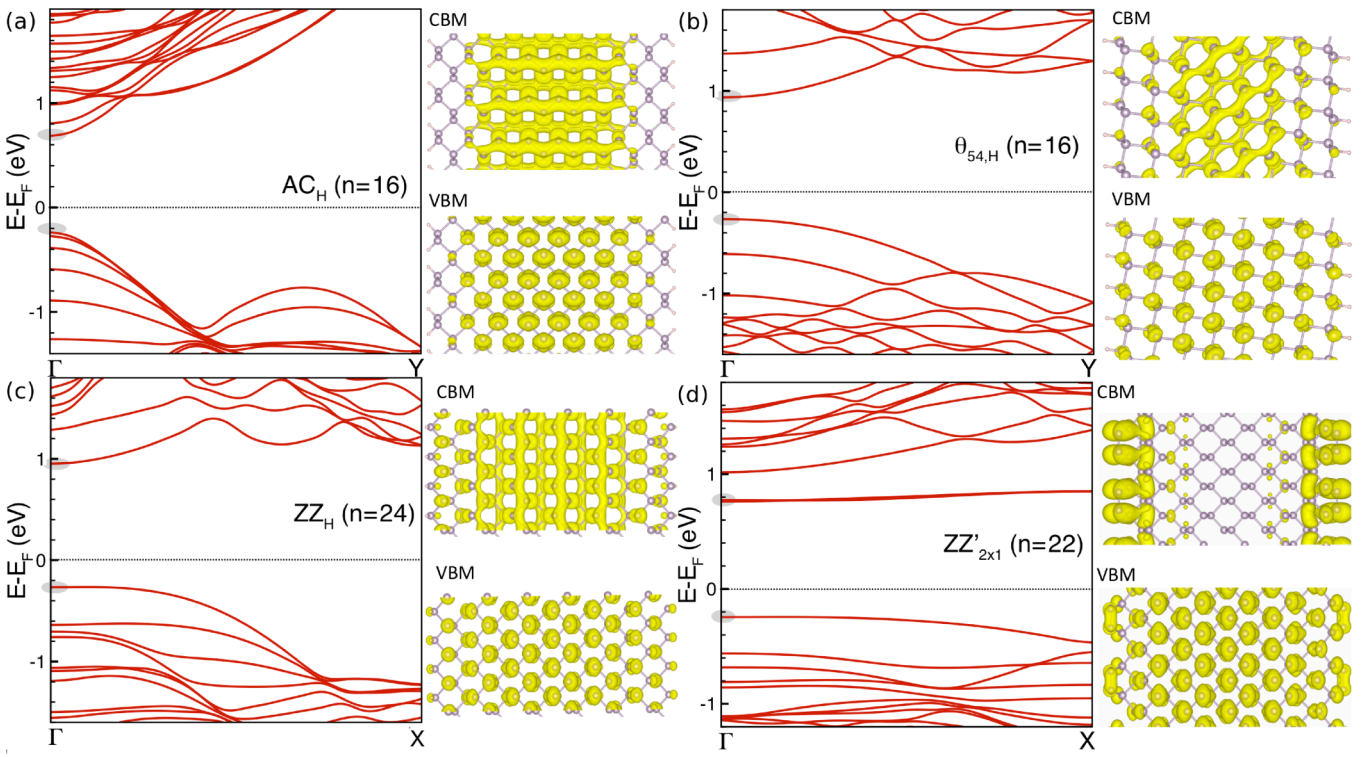

FIG. 6. (Color online) Band structures of (a) AC_H, (b) $\theta_{54,H}$, (c) ZZ_H, and (d) ZZ'_{2x1} nanoribbons. Ribbon sizes n are assigned as per the indexing scheme in Figs. 2 and 3. Also displayed here are the partial charge densities (at arbitrary isosurface levels) of the valence band maximum (VBM) and the conduction band minimum (CBM), which are marked by gray ellipses in the band-structure plot.

[29]. While our calculations thus suffer from known DFT band-gap problems, qualitative trends for changes in band gap with ribbon width and edge termination are expected to be more reliable.

Figure 5 displays the calculated DFT fundamental gaps for all semiconducting ribbons as a function of ribbon width. Examples of band structures for ribbons with thermodynamically preferred edge terminations identified in the phase diagram in Fig. 4(b), namely, AC_H, $\theta_{54,H}$, ZZ_H, and ZZ'_{2x1} ribbons, are displayed in Fig. 6. The ZZ, ZZ′, and ZZ'_{1H} ribbons are metallic and are not considered further; band-structure plots for these cases are displayed in the Supplemental Material [25]. As seen from Fig. 5 all hydrogenated ribbons have direct band gaps at Γ that are larger than pristine phosphorene and these gaps decrease systematically with increasing ribbon width, which is a sign of quantum confinement of carriers. Of the ribbons with bare edges, ZZ'_{2x1} ribbons also have direct band gaps at Γ (except for very narrow ribbons $\lesssim$1 nm) that are larger than pristine phosphorene; the AC ribbons, however, have indirect gaps that are smaller than phosphorene due to the appearance of a midgap state arising from dangling bonds at the ribbon edge (see Supplemental Material [25], Fig. S2). For AC_H, $\theta_{54,H}$, ZZ_H, and ZZ'_{2x1} ribbons, in particular, we see from Fig. 5 that for a specific width, the band gaps, E_g, are consistently ordered as $E_{g,ZZ_H} > E_{g,\theta_{54,H}} > E_{g,ZZ'_{2x1}} > E_{g,AC_H}$. Thus, by choosing the edge termination (tuning temperature and H partial pressure) and ribbon width, it should be possible to produce stable nanoribbons with a range of tailored band gaps. Interestingly, it might also be possible to synthesize metastable ribbons (AC ribbons)—with band gaps that are smaller than phosphorene—or even metallic ribbons, although it should be noted that all such ribbons have dangling bonds at the edges, which, being reactive, make the edge prone to contamination; it might be possible though to envision other edge functionalization strategies to chemically stabilize the edges and achieve these properties.

IV. CONCLUSIONS

In conclusion, we have presented a detailed study of PNRs with low Miller index edges accounting for both bare and hydrogenated edge terminations. From *ab initio* thermodynamics calculations, we have identified three hydrogenated edges, namely, the hydrogenated armchair (AC_H), 54° ($\theta_{54,H}$), and zigzag (ZZ_H) edges that are thermodynamically preferred at low temperatures over a wide range of hydrogen partial pressures. At elevated temperatures, the bare dimer-reconstructed zigzag edge (ZZ'_{2x1}) edge is thermodynamically preferred. Ribbons with fully passivated edges (no dangling bonds) are found to be semiconducting with band gaps that vary inversely with ribbon width due to quantum confinement. Ribbons with bare or partially passivated edges either have metallic edges or are semiconducting with band gaps that are smaller than their hydrogenated counterparts due to the appearance of midgap edge states. Thus, by selecting for stable ribbon edge terminations via control over temperature and partial pressure of hydrogen, and by controlling the ribbon width, it should be possible to tune the band gap up to ∼0.5 eV in excess of the gap of a phosphorene monolayer. Further investigations are needed to study the energetics of high Miller index edges for producing a complete Wulff plot for phosphorene. Also, additional work is required to study the effect of passivation by a variety of atomic species and functional groups on the thermodynamics and electronic structure of PNRs. These and other issues will be reported in future work.

ACKNOWLEDGMENTS

A.R. acknowledges funding from the University of Massachusetts, Amherst NSF-MRSEC on Polymers, DMR-0820506, and computational support from the Massachusetts Green High Performance Computing Center.

[1] A. Brown and S. Rundqvist, Acta Crystallogr. **19**, 684 (1965).
[2] L. Cartz, S. R. Srinivasa, R. J. Riedner, J. D. Jorgensen, and T. G. Worlton, J. Chem. Phys. **71**, 1718 (1979).
[3] A. Morita, Appl. Phys. A: Mater. Sci. Process. **39**, 227 (1986).
[4] H. Asahina and A. Morita, J. Phys. C: Solid State Phys. **17**, 1839 (1984).
[5] L. Li, Y. Yu, G. J. Ye, Q. Ge, X. Ou, H. Wu, D. Feng, X. H. Chen, and Y. Zhang, Nat. Nanotech. **9**, 372 (2014).
[6] S. Koenig, R. Doganov, H. Schmidt, A. Castro Neto, and B. Özyilmaz, Appl. Phys. Lett. **104**, 103106 (2014).
[7] H. Liu, A. T. Neal, Z. Zhu, Z. Luo, X. Xu, D. Tománek, and P. D. Ye, ACS Nano **8**, 4033 (2014).
[8] A. S. Rodin, A. Carvalho, and A. H. Castro Neto, Phys. Rev. Lett. **112**, 176801 (2014).
[9] G. Seifert and T. Frauenheim, J. Korean Phys. Soc. **37**, 89 (2000).
[10] I. Cabria and J. Mintmire, Europhys. Lett. **65**, 82 (2004).
[11] H. Guo, N. Lu, J. Dai, X. Wu, and X. C. Zeng, J. Phys. Chem. C **118**, 14051 (2014).
[12] V. Tran and L. Yang, Phys. Rev. B **89**, 245407 (2014).
[13] A. Carvalho, A. S. Rodin, and A. H. Castro Neto, arXiv:1404.5115.
[14] X. Peng, Q. Wei, and A. Copple, arXiv:1404.5995.
[15] X. Peng and Q. Wei, arXiv:1405.0801.
[16] G. Kresse and J. Furthmüller, J. Comp. Mater. Sci. **6**, 15 (1996); Phys. Rev. B **54**, 11169 (1996).
[17] P. E. Blöchl, Phys. Rev. B **50**, 17953 (1994).
[18] G. Kresse and D. Joubert, Phys. Rev. B **59**, 1758 (1999).
[19] J. P. Perdew, K. Burke, and M. Ernzerhof, Phys. Rev. Lett. **77**, 3865 (1996).
[20] F. Xia, H. Wang, and Y. Jia, Nat. Commun. **5**, 5548 (2014).
[21] J. Rogal and K. Reuter, in *Experiment, Modeling and Simulation of Gas-Surface Interactions for Reactive Flows in Hypersonic Flights*; Educational Notes RTO-EN-AVT-142, Neuilly-sur-Seine (2007), pp. 2-1–2-18.
[22] K. Reuter and M. Scheffler, Phys. Rev. B **65**, 035406 (2001).
[23] K. Johnston, M. R. Castell, A. T. Paxton, and M. W. Finnis, Phys. Rev. B **70**, 085415 (2004).
[24] NIST Chemistry WebBook, NIST Standard Reference Database Number 69, edited by P. J. Linstrom and W. G. Mallard,

National Institute of Standards and Technology, Gaithersburg, MD, 20899, http://webbook.nist.gov/chemistry/, accessed April 2014.

[25] See Supplemental Material at http://link.aps.org/supplemental/10.1103/PhysRevB.90.085424 for a comparison of *ab initio* and experimental chemical potentials for H_2 gas and band-structure plots for nanoribbons.

[26] Ø. Prytz and E. Flage-Larsen, J. Phys.: Condens. Matter **22**, 015502 (2010).

[27] Y. Du, C. Ouyang, S. Shi, and M. Lei, J. Appl. Phys. **107**, 093718 (2010).

[28] J. Qiao, X. Kong, Z.-X. Hu, F. Yang, and W. Ji, Nat. Commun. **5**, 4475 (2014).

[29] A. Ramasubramaniam, Phys. Rev. B **86**, 115409 (2012).